

# Free Radical Formation by the Peroxidase-like Catalytic Activity of $MFe_2O_4$ ( $M = Fe, Ni$ and $Mn$ ) Nanoparticles

Ana Carolina Moreno Maldonado<sup>a,‡</sup>, Elin L. Winkler<sup>a,b,‡</sup>, Mariana Raineri<sup>b</sup>, Alfonso Toro Córdova<sup>c</sup>, Luis M. Rodríguez<sup>b,†</sup>, Horacio E. Troiani<sup>a,d</sup>, Mary Luz Mojica Piscioti<sup>b,†</sup>, Marcelo Vasquez Mansilla<sup>b</sup>, Dina Tobia<sup>b</sup>, Marcela S. Nadal<sup>b</sup>, Teobaldo E. Torres<sup>b</sup>, Emilio De Biasi<sup>b</sup>, Carlos A. Ramos<sup>b</sup>, Gerardo F. Goya<sup>c,e</sup>, Roberto D. Zysler<sup>a,b</sup>, Enio Lima Jr.<sup>b,\*</sup>

<sup>a</sup> Instituto Balseiro, Universidad Nacional de Cuyo – CNEA, 8400, S. C. Bariloche, RN, Argentina.

<sup>b</sup> Instituto de Nanociencia y Nanotecnología, CNEA, CONICET, Centro Atómico Bariloche, 8400, S. C. Bariloche, Argentina.

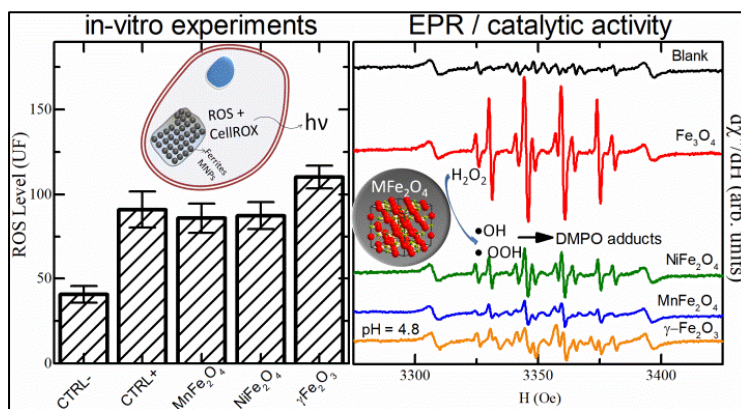
<sup>c</sup> Instituto de Nanociencia de Aragón (INA), Universidad de Zaragoza, 50018 Zaragoza, Spain.

<sup>d</sup> Grupo de Caracterización de Materiales y Óxidos No-Estequiométricos, Gerencia de Investigación Aplicada, CNEA, CONICET, Centro Atómico Bariloche, 8400, S. C. Bariloche, Argentina.

<sup>e</sup> Departamento de Física de la Materia Condensada, Facultad de Ciencias, Universidad de Zaragoza, 50009 Zaragoza, Spain.

**ABSTRACT.** Ferrite Magnetic Nanoparticles (MNPs) have peroxidase-like activity and thus catalyze the decomposition of  $H_2O_2$  producing reactive oxygen species (ROS). Increasingly important applications of these Ferrite MNPs in biology and medicine require that their morphological, physicochemical and magnetic properties need to be strictly controlled. Usually, the tuning of their magnetic properties

is achieved by the replacement of the Fe by other 3d metals, such as Mn or Ni. Here, we studied the catalytic activity for ferrite MNPs ( $MFe_2O_4$ ,  $M = Fe^{2+}/Fe^{3+}$ , Ni, Mn) with mean diameter ranging from 10 to 12 nm. Peroxidase-like activity was studied by Electron Paramagnetic Resonance (EPR) using the spin-trap DMPO at different pHs (4.8, 7.4) and temperatures (25°C, 40°C). We identified an enhanced amount of the hydroxyl ( $\bullet OH$ ) and perhydroxyl ( $\bullet OOH$ ) radicals for all samples, compared to a blank solution. Quantitative studies show that [ $\bullet OH$ ] is the dominant radical formed for  $Fe_3O_4$ , which is strongly reduced with the concomitant oxidation of  $Fe^{2+}$  or its substitution (Ni or Mn). A comparative analysis of the EPR data against in vitro production of ROS in microglial BV2 cell culture provided additional insight regarding the catalytic activity of ferrite MNPs, which should be considered if biomedical uses are intended. Our results contribute to a better understanding of the role played by different divalent ions in the catalytic activity of Ferrite nanoparticles, which is very important concerning their use in biomedical applications.



## Introduction

Ferrite Magnetic Nanoparticles (MNPs) are currently being used in many different clinical protocols approved by regulatory agencies like the FDA.<sup>1</sup> Mixed-ferrites with the general formula  $M_xFe_{3-x}O_4$  (i.e., incorporating other 3d metallic ions within the spinel structure) are of interest to biomedicine since their magnetic properties can be adjusted for specific purposes, e.g. to serve as MRI contrast agents<sup>2</sup> or to tune the heating response in magnetic hyperthermia.<sup>3</sup>

The peroxidase-like activity of the bulk iron oxides catalyzed by Fenton-based reactions involves the decomposition of hydrogen peroxide ( $H_2O_2$ ) into reactive oxygen species (ROS) such as the radicals  $\bullet OH$  and  $\bullet OOH$ .<sup>4</sup> Hence, for simplification, here we consider the peroxidase-like activity of MNPs as the catalytic activity that involves the decomposition of  $H_2O_2$  into  $\bullet OH$  and  $\bullet OOH$  radicals. This peroxidase-like activity of iron oxides has many well-documented differences with the enzymatic activity of actual peroxidases regarding their dependence on pH, temperature and  $H_2O_2$  concentration.<sup>5,6</sup> Nevertheless, the enzymatic-like activity of natural iron oxides and hydroxides containing  $Fe^{2+}$  and  $Fe^{3+}$  is known to play a significant role in several geological-dependent biological processes of plants and microorganisms.<sup>7</sup>

In 2007, Gao *et al.*<sup>8</sup> measured the peroxidase-like catalytic activity of magnetite ( $Fe_3O_4$ ) nanoparticles under different experimental conditions, reporting a strong increase in the catalytic activity with: a) decreasing nanoparticle size, suggesting a surface-related effect, and b) increasing  $Fe^{2+}/Fe^{3+}$  ratios, indicating an active role of ferrous iron. These results were immediately recognized as extremely relevant because of the ubiquity of iron-oxide MNPs in medicine and biology protocols.<sup>9-11</sup> On the other hand,

Gumpelmayer *et al.*<sup>12</sup> have recently reported that removing free iron ions from the surface of  $Fe_3O_4$  nanoparticles with a Chelex Buffer eliminates their intrinsic peroxidase-like activity. It is important to note that these two works mentioned above were done using commercial  $Fe_3O_4$  MNPs, and provide very few details about their composition and surface properties. Moreover, in both cases, the data on the peroxidase-like activity was relative to the oxidation of a chromogenic substrate. Although recent works have provided a better characterization of the ferrite MNPs and have linked the MNP-coatings to their peroxidase-like activity,<sup>13</sup> quantitative data of ROS production from well-characterized ferrite nanoparticles under different physiological conditions are still lacking. In particular, further experimental work is required to assess whether  $Fe_3O_4$  nanoparticles are capable of triggering peroxidase-like catalytic mechanisms *in vitro* and *in vivo*.

It is known that for bulk materials or nanoparticles, the incorporation of 3d transition metals (specially  $Co^{2+}$ ,  $Mn^{2+}$  and  $Ni^{2+}$ ) into the tetrahedral and octahedral sites of the spinel structure strongly affects the reactivity towards  $H_2O_2$ .<sup>14</sup> Incorporation of Co or Mn yields a measurable increase in the formation of the  $\bullet OH$  species, while  $Ni^{2+}$  ions inhibit this reaction.<sup>14-17</sup> Using a luminol-based chemiluminescent reaction, Shi *et al.*<sup>18</sup> found that  $CoFe_2O_4$  ferrite nanoparticles were able to catalyze  $H_2O_2$  decomposition. Yet, the limitation of this non-specific technique is that it cannot be used to differentiate among the radical species produced in the reaction, thus hindering their quantification.

The relevance of the catalytic activity of ferrite nanoparticles has been clearly illustrated by Clerc *et al.*<sup>19</sup>, who proposed a dual-effect in oncologic treatments by combining the peroxidase-like activity of ferrite nanoparticles in the acidic pH of

lysosomes, with their heating ability for magnetic fluid hyperthermia (MFH), a synergistic approach that could improve apoptosis of target cells.

Electron Paramagnetic Resonance (EPR) is perhaps the most sensitive measurement technique used to identify and quantify individual free radical species.<sup>20-26</sup> Due to the high reactivity and short half-life of the free radicals, this technique requires the use of a diamagnetic 'spin-trap' compound, such as the 5,5-Dimethyl-1-pyrroline N-oxide (DMPO), that generates a more stable paramagnetic radical adducted species, which can be readily detected. The EPR technique has been already used to study the peroxidase-like activity of Fe<sub>3</sub>O<sub>4</sub> nanoparticles in the decomposition rate of H<sub>2</sub>O<sub>2</sub> at some physiological pHs.<sup>27</sup> The authors observed a substantial increment of •OH formed by the nanoparticles at pH 4.8 (similar to lysosomal conditions), and almost null catalytic activity of the nanoparticles at pH of 7.4 (similar to the cytoplasm of healthy cells). More recently, EPR spectroscopy using DMPO was applied to elucidate the main mechanisms of the Fenton-like and Haber-Weiss-like catalytic reactions. These studies were able to associate the formation of the free radical •OH to the activity of Fe<sup>2+</sup> and of •OOH with the activity of Fe<sup>3+</sup>.<sup>4</sup> Although DMPO is a good tool to study the formation of the free radical •OH (with a lifetime in the order of several minutes), it can also be used to identify the free radical •OOH. Nevertheless, the analyses of the later one needs to be carefully adjusted since the amounts of •OOH (as determined by the adduct DMPO-OOH) are underestimated because it has a relative slow kinetic of formation and a short half-life (50 s).<sup>28-30</sup>

In this work, we have focused in the role of Fe<sup>2+</sup> on the peroxidase-like catalytic activity of different ferrite nanoparticles with general formula M<sub>x</sub>Fe<sub>3-x</sub>O<sub>4</sub> (M = Fe, Ni, Mn) using

EPR and the spin trap DMPO. We identified the formation of the free radicals •OH and •OOH from H<sub>2</sub>O<sub>2</sub> generated under different conditions of pH (4.8 and 7.4) and temperature (25 °C and 40 °C). The absolute quantification was performed for the radical •OH, which is the dominant species in the catalytic activity of the Fe<sup>2+</sup> ion. A comparative study among the nanoparticles of the radical •OOH formation was also performed. Since the passivation of the ferrite particle surface can play a major role in the catalytic activity,<sup>31</sup> we have also analyzed the influence of two chelating agents with distinct interaction properties in respect to the metallic ions.

To compare the peroxidase-like activity among the samples we focused on the concentration of the free radical •OH ([•OH]). The nanoparticle morphology and composition were characterized by Transmission Electron Microscopy (TEM) and X-ray Photoemission Spectroscopy (XPS), respectively. The amount of the free radical •OH ([•OH]) produced is related to the composition, specifically to the Fe<sup>2+</sup>/Fe ratio in the ferrite. Finally, the results obtained from the EPR experiments were contrasted with in vitro experiments in BV2 cells through fluorescence to assess the peroxidase-like activity of the Dextran-coated MNPs.

## Experimental Methods

### Materials

The following chemical reagents were used in the synthesis and functionalization of the nanoparticles. The organometallic precursors Fe<sup>3+</sup> acetylacetonate (Fe(acac)<sub>3</sub>, 97 %), Ni<sup>2+</sup> acetylacetonate (Ni(acac)<sub>2</sub>, 95 %) and Mn<sup>2+</sup> acetylacetonate (Mn(acac)<sub>2</sub>, technical grade), 1,2-octanediol (98 %), oleic acid (analytical standard), oleylamine (70 %), benzyl ether (98 %), methanol (reag. Ph. Eur.), ethanol (96 %), acetone (reag. Ph Eur.), chloroform (> 99

%), toluene (99.8 %), Dextran (analytical standard, mw 12000) and ammonium hydroxide (27 %) were purchased from Sigma-Aldrich (USA). The hydrochloric acid (HCl, 37 %), iron chloride ( $\text{FeCl}_3 \cdot 6\text{H}_2\text{O}$ , 97 %), potassium phosphate ( $\text{K}_3\text{PO}_4$ , 98 %) and potassium thiocyanate (KCSN, > 99.9 %) used in the determination of the nanoparticle composition by UV analysis; and the 5,5-Dimethyl-1-pyrroline N-oxide (DMPO, > 97 %) and dimethyl sulfoxide (DMSO, > 99 %) used in EPR experiments, as well as Tert-Butyl hydroperoxide solution (Luperox® TBH70X, 70% in water) used for in vitro experiments were also purchased at Sigma-Aldrich. Quartz tubes (2 mm of thickness) for Q-band used in the EPR experiments were purchased from Wilmar (USA). A MgO crystal doped with  $\text{Mn}^{2+}$  ions was selected among other crystals to have nearly zero  $\text{Cr}^{3+}$  impurities, thus providing clean central spectra while providing a calibrating intensity and line position reference. Phosphate Buffered Saline (PBS), Fetal Bovine Serum (FBS), Dulbecco's Modified Eagle's Medium (DMEM) and CellROX® Green Reagent were purchased from ThermoFisher Scientific (USA).

### Synthesis of the Nanoparticles

The magnetic nanoparticles used in this work were synthesized through the high-temperature decomposition of  $\text{Fe}(\text{acac})_3$ ,  $\text{Ni}(\text{acac})_2$  and  $\text{Mn}(\text{acac})_2$  precursors, following the synthesis route described elsewhere.<sup>32,33</sup> The nanoparticles obtained with this procedure are coated mainly by oleic acid and partially by oleylamine. The organic surface coating was removed in order to disperse the nanoparticles in water. To perform this step, the nanoparticles were dispersed in methanol for 8 hours at 40 °C and afterwards in acetone for 48 hours at 40 °C. After this treatment, the absence of the coating of oleic acid and oleylamine was verified by Fourier-Transform Infrared spectroscopy (FTIR), as shown in Figure S1

presented in supplementary information. Afterwards, the chemically etched nanoparticles were coated with dextran for in vitro experiments. For this purpose, the nanoparticles were dispersed with ten times the mass of dextran in an ammonium hydroxide solution (0.1 N, pH = 11) during 48 hours under stirring, followed by magnetic separation and washing several times with ultrapure water. An oxidized  $\text{Fe}_3\text{O}_4$  MNPs sample was prepared by following the previous methodology without using Dextran. The magnetic nanoparticles made of  $\text{Fe}_3\text{O}_4$ , as well as its oxidized counter-part ( $\gamma\text{-Fe}_2\text{O}_3$ ),  $\text{Ni}_x\text{Fe}_{3-x}\text{O}_4$  and  $\text{Mn}_x\text{Fe}_{3-x}\text{O}_4$  were labeled as Fe-MNP sample, oxFe-MNP sample, Ni-MNP sample and Mn-MNP sample, respectively.

### Characterization of the Nanoparticles

The morphology and size dispersion of the nanoparticles were analysed from Transmission Electron Microscopy (TEM) images taken in a F20 TECNAI microscope operating at 200 kV. The analysis of the nanoparticle surface coating was done by Fourier-Transform Infrared spectroscopy (FTIR) performed in a Spectra Two spectrometer (Perkin Elmer), using a uATR optical configuration.

To obtain the oxidation state of the metallic ions in the nanoparticles, X-ray photoelectron spectroscopy (XPS) measurements were performed with a SPECS spectrometer, using a 150 mm Phoibos hemispherical analyzer in the energy range of Al-K $\alpha$  (1486.6 eV) and a chamber pressure of  $10^{-10}$  mBar. In order to determine the  $\text{Fe}^{2+}/\text{Fe}$  ratio in each sample, their XPS spectra in the Fe-2p energy range was analysed. The fitting procedure used for the Fe-2p<sub>3/2</sub> peak for each sample was similar to that reported by Grosvenor et al.<sup>34</sup> In this way, the binding energy for each sample was calibrated using the C1s peak position with the reference value of 284.8 eV; a Shirley-type background was used in the fitting in order to remove most of the extrinsic loss

structure; and the Fe-2p<sub>3/2</sub> envelope was fitted using multiplets (3 peaks corresponding to Fe<sup>2+</sup> and 4 for the Fe<sup>3+</sup> in the ferrite structure), with correlations among the binding energy and area of the peaks. High-energy peaks corresponding to surface structures and shake-up-related satellites were also added. The Ni/Fe and Mn/Fe ratios were obtained by analysing the XPS spectra of the samples in the Fe-Ni-Mn 3p energy range. In this way, the area of each peak referent to the respective element was obtained by numerical integration<sup>35-37</sup> and the Ni/Fe and Mn/Fe ratios were calculated taking into account the corresponding photoionization cross section in this energy range<sup>38</sup>.

Fe<sup>3+</sup> and total Fe contents in the nanoparticles were obtained by UV-visible (UV-vis) Spectrophotometry following the procedure described below. The as-synthesized particles were washed several times with toluene to remove the excess of oleic acid followed by a wash in HCl (6 N) for 10 min at 60 °C, and then placed into two tubes. To obtain the total iron concentration, one of the tubes was incubated with 5 µL of 3% H<sub>2</sub>O<sub>2</sub> with the aim to oxidize all Fe<sup>2+</sup> to Fe<sup>3+</sup>; the second tube was incubated with 5 µL of ultrapure water to determine the initial Fe<sup>3+</sup> amount. Iron standard solutions were prepared by dissolving FeCl<sub>3</sub>·6H<sub>2</sub>O in ultrapure water (0-150 ppm) and processed for total iron determination. Finally, Fe<sup>3+</sup> concentration was determined by adding 400 µL of 0.5 M potassium thiocyanate (KSCN) and measuring the absorbance of the red complex at 480 nm. Since the Fenton reaction can catalyze KSCN oxidation in acidic media,<sup>39</sup> the H<sub>2</sub>O<sub>2</sub> concentration was carefully selected. In our experiments, after increasing the H<sub>2</sub>O<sub>2</sub> concentration by a factor of ten, a decrease in the sample absorbance was observed, possibly due to KSCN oxidation. In contrast, absorbance of standard solutions was not altered when increasing H<sub>2</sub>O<sub>2</sub>, probably because Fenton reaction depends

mainly on the Fe<sup>2+</sup>/ H<sub>2</sub>O<sub>2</sub> ratio and we used Fe<sup>3+</sup> to create the calibration curve. To assess the performance of the method, pure magnetite ([Fe<sup>3+</sup>] = 66.6%) was introduced as a standard to validate our results. The absorbance spectra of Fe<sup>2+</sup>, Ni<sup>2+</sup> and Mn<sup>2+</sup>, before and after oxidation were also recorded.

#### Catalytic Activity Measured by EPR

Electron paramagnetic resonance measurements were performed in an ELEXSYS II-E500 spectrometer (Bruker) with an X-band resonant cavity (9.4 GHz) at specific temperatures of 25°C and 40°C. The spectra were acquired with an attenuation of 10 dB (20 mW microwave power) and 1 Oe of amplitude of the modulation field. The solutions for the EPR experiments were prepared by dispersing 120 µg of nanoparticles in 200 µL of an acetate buffer solution (pH = 4.8), or in phosphate buffer solution (pH = 7.4). In each solution, 50 µL of a DMPO/DMSO solution with DMSO concentration of 0.33 g/mL (0.56 M) and 10 µL of H<sub>2</sub>O<sub>2</sub>-30 % were added (0.49 M). The starting point of the reaction was assumed to be the moment the H<sub>2</sub>O<sub>2</sub> was added. In order to quantify the amounts of the free radicals, the EPR spectrum of each solution in a quartz tube was measured simultaneously with the MgO pattern crystal, doped with a known concentration of Mn<sup>2+</sup> attached to the tube. The dependences of the obtained EPR spectra with the microwave power for 15 dB, 20 dB, 25 dB and 30 dB were recorded in order to analyze the effect of the signal saturation and deviations from the expected linear dependence at lower attenuations and were considered for the quantification. The collected spectra were fitted with the software SPIN® from Bruker using the same procedure for all measurements in the following order: first, the ferromagnetic resonance of the ferrite nanoparticles was subtracted and then the resonance lines were adjusted with the hyperfine parameters of five different species. In order to identify each

species, we used the fitted values of hyperfine constant in the Spin Trap database of the National Institute of Environmental Health Sciences – NIEHS, USA (<https://tools.niehs.nih.gov/stdb/index.cfm>). The •OH, •OOH, •CH<sub>3</sub> and •N free radical concentrations were obtained by comparing the EPR fitted spectrum intensities of every species with the intensity of the MgO/Mn<sup>2+</sup> pattern, as reported elsewhere.<sup>40,41</sup>

#### In vitro tests of ROS production

The in vitro production of ROS by the MNPs was tested in BV2 cells (mouse, C57BL/6, microglia) from ATCC (Manassas, VA, USA). Cells were routinely cultured in Dulbecco's Modified Eagle Medium supplemented with 10% fetal bovine serum at 37 °C in a 5% CO<sub>2</sub> atmosphere. Control groups consisted of untreated cells (negative control) and cells treated with 10 or 20 μM of tert-butyl hydroperoxide (TBHP) as positive control. Experimental groups were made of cells treated with Fe<sub>3</sub>O<sub>4</sub>, NiFe<sub>2</sub>O<sub>4</sub> or Mn<sub>0.66</sub>Fe<sub>2.34</sub>O<sub>4</sub> nanoparticles at concentration of 50 μg/mL. Both hydroperoxide and MNPs concentrations were tested before and proved to be non-cytotoxic. The quantification of ROS produced in vitro was performed with cells seeded in 96-well plates at a density of 4 x 10<sup>3</sup> cells/well, allowing cells to attach overnight before incubating with the different treatments for 24 h. For the evaluation of ROS production at 40 °C, cells were incubated the last hour at this temperature. After this time, CellROX reagent was added at final concentration of 50 μM and incubated for another 30 minutes at 37 °C. Then, cells were washed 3x with PBS and fluorescence was measured with a Synergy HT plate reader (Biotek, Winooski, VT, USA) using a 485/20 nm excitation and 530/25 nm emission filter set, using the comparative Relative Fluorescence Units (RFU).

For the statistical analysis of the ROS determination in vitro results, InfoStat software (Universidad Nacional de Córdoba,

Argentina) was used. Statistics were performed using one-way ANOVA and Tukey multiple comparisons test when applicable. Differences were considered significant if p<0.05. Population statistics are presented as mean ± standard error of the mean.

## Results

### Morphology and Composition

The peroxidase-like catalytic activity of MNPs is known to be highly dependent on the surface area and the particle composition. Therefore, a proper nanoparticle characterization is essential in order to understand the dynamics of free radical formation. Figure 1 shows representative TEM images of Fe-MNP, Mn-MNP and Ni-MNP, where different shapes can be observed (rounded for Fe-MNP and a mixture of rounded and faceted for Ni-MNP and Mn-MNP). Size histograms were obtained from the TEM images (right panels, Figure 1), and then fitted with a Gaussian distribution to obtain the mean diameters (<d>) and standard deviations (σ) that are given in Table 1.

When considering the Fenton based reactions, the Fe<sup>2+</sup>/Fe molar ratio in the nanoparticles is critical in order to understand the catalytic activity of the samples<sup>1-5</sup>. For this reason, we used X-ray Photo-emission Spectroscopy (XPS) to analyze changes in the oxidative state of iron in the nanoparticle after the incorporation of Ni and Mn in the spinel structure. Table 1 gives the Fe<sup>2+</sup>/Fe ratio, as well as the Mn/Fe and Ni/Fe ratios, obtained from the XPS spectra. Figures S2 and S3 in the supplementary information show the spectra with the corresponding fitting curves, together with a table with the fitting parameters for the spectra Fe-2p<sup>3/2</sup> and 3p (Figure S4 in the supplementary information), respectively.

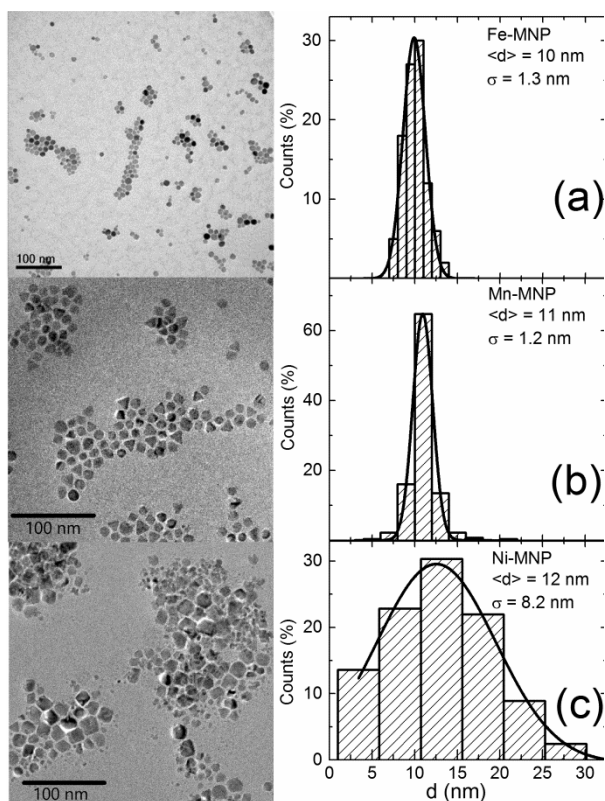


**Figure 1.** Representative Transmission Electron Microscopy (TEM) images for samples (a): Fe-MNP, (b): Mn-MNP and (c): Ni-MNP. Right panels: the respective diameter histogram fitted with a Gaussian distribution and the obtained values for the mean diameter  $\langle d \rangle$  and dispersion  $\sigma$ .

From other studies it is known that system prepared in similar way that our samples present a ferrite structure. Thus, we consider a general formula of  $MFe_2O_4$  for samples Fe-

MNP, Mn-MNP and Ni-MNP, and  $Fe_{2.67}O_4$  for the sample oxFe-MNP, despite a small stoichiometry deviation with oxygen vacancies may take place. Thus, according to the XPS analysis, the complete formula of the samples can be written as: Fe-MNP =  $Fe^{2+}_{0.81}Fe^{3+}_{2.19}O_4$ ; Mn-MNP =  $Mn_{0.33}Fe^{2+}_{0.61}Fe^{3+}_{2.06}O_4$  and Ni-MNP =  $Ni_{0.84}Fe^{2+}_{0.30}Fe^{3+}_{1.86}O_4$ . To provide further support for the obtained data, the  $Fe^{2+}/Fe$  molar ratios were also obtained by UV-visible spectrophotometric quantification of  $Fe^{3+}$  ions by of the  $Fe^{3+}$ -thiocyanate complex formation ( $\lambda_{\text{absorption}} \approx 465\text{ nm}$ ), after particle dissolution in HCl 6 N (see Table 1). The UV-visible spectra of the different transition metal ions are given in Figure S5 of the supplementary information. For total Fe quantification in each sample, a strong oxidation process was induced by adding  $H_2O_2$  to the solution prior  $Fe^{3+}$  quantification.  $Fe^{2+}/Fe$  ratios obtained from the Fe-thiocyanate UV-visible spectrophotometric are in good agreement with the values obtained from the XPS spectroscopy. Both measurements show a decrease in  $Fe^{2+}$  content after Mn and Ni substitution, indicating a preferential substitution of  $Fe^{2+}$  by Mn and Ni. In addition, oxidation of Fe-MNP samples (exposed 48 h to an alkaline aqueous solution of  $pH = 12$ ,  $40^\circ C$ ) resulted in almost complete oxidation of  $Fe^{2+}$ , as determined by the  $Fe^{3+}$ -thiocyanate method, showing a  $Fe^{2+}/Fe$  ratio of about 0.07.

**Table 1.** Morphological and compositional parameters of the samples. The standard errors in the compositional analyzes are given in the parentheses and it is in references to the last digit

Technique	Parameter	Sample			
		Fe-MNP	Mn-MNP	Ni-MNP	oxFe-MNP
TEM*	$\langle d \rangle$ (nm)	10	11	12	10
	$\sigma$ (nm)	1.3	1.2	8.2	1.3
XPS	Mn/Fe	-	0.12 (2)	-	-

	Ni/Fe	-	-	0.40 (1)	-
	Fe <sup>2+</sup> /Fe	0.27 (2)	0.23 (2)	0.14 (2)	-
Fe <sup>3+</sup> -thiocyanate method	Fe <sup>2+</sup> /Fe	0.27 (3)	0.23 (3)	0.09 (4)	0.07 (4)

\*  $\langle d \rangle$  is the main diameter and  $\sigma$  is the dispersion obtained from the respective histogram fit with a Gaussian distribution.

### Catalytic Activity by EPR

The catalytic activity of the nanoparticles in buffer solutions (pH = 4.8 and pH = 7.4) after addition of H<sub>2</sub>O<sub>2</sub> was recorded by EPR spectroscopy at 40°C with the addition of the spin-trap DMPO in DMSO to detect and identify the free radicals formed in the peroxidase reaction. Figure 2 shows the EPR spectra measured at 40°C in acetate buffer solution (pH = 4.8) for the Fe-MNP, Ni-MNP, Mn-MNP samples and the oxidized form of Fe-MNP (oxFe-MNP). Here, nanoparticle activities were referred to the blank sample spectra, which correspond to the same solutions but without the nanoparticles. It should be noticed that intensities in EPR spectra of the nanoparticle containing solutions are larger than blank samples in every case (Figure 2). Moreover, a remarkable enhancement of the EPR intensity was observed for the dispersion containing the Fe<sub>3</sub>O<sub>4</sub> MNPs (Fe-MNP). After a detailed analysis, it was observed that each EPR spectrum was composed of the resonance signals of five different paramagnetic species (Figure 3). The contributions detected are: i) the outer lines corresponding to the central resonance lines of the Mn<sup>2+</sup> ions in the MgO

crystal;<sup>42</sup> ii) the DMPO/•OH free radical spectrum composed of four resonance lines with a 1:2:2:1 intensity ratio that results from the splitting of the resonance line due to the hyperfine interaction of the electronic spin with the nuclear spin of the nitrogen and the hydrogen ions; iii) The DMPO/•OOH radical spectrum with six lines resulting from the convolution of 12 resonances, corresponding to the hyperfine interaction of the electron spin with a nitrogen and two hydrogen ions; iv) the DMPO/•CH<sub>3</sub> radical contribution, probably resulting from a secondary reaction of the DMSO with the H<sub>2</sub>O<sub>2</sub> or the free radical •OH; and v) three broader lines that are related to the interaction of the electron spin of oxidized DMPO with a nitrogen ion (DMPO/•N). Table 2 summarizes the hyperfine parameters obtained for each radical in all spectra. It is worth noting that the different paramagnetic species can be well characterized with the  $g$ ,  $H_{SF}$  and  $w$  parameters that remain unchanged in the different experimental conditions, for all samples. Only changes in areas were observed. Finally, the cavity and Quartz tube signal only were measured and found to have only a very small and very broad contribution, which does not interfere with the free radical contribution.

**Table 2.** EPR parameters obtained from the fitting of the EPR spectra for the different samples.  $g$  = gyromagnetic ratio;  $w$  = linewidth; LS = line shape coefficient (1 for a Lorentzian distribution and 0 for a Gaussian one);  $H_{SF}$  is the Hyperfine of Mn<sup>2+</sup>/MgO for  $I = 5/2$ ;  $H_{SF}^N$  and  $H_{SF}^H$  are the hyperfine coupling field between the electronic spin and the nuclear spins of the N and H ions, respectively. The standard error is given in the parentheses and it is in references to the last digit.



	Mn <sup>2+</sup> /MgO	•OH	•CH <sub>3</sub>	•OOH	•N
G	2.0005(3)	2.0023(3)	2.0024(3)	2.0023(3)	2.0023(3)
W [Oe]	4.3(5)	1.4 (2)	1.4 (2)	1.5 (2)	2.1 (4)
LS	0.2 (2)	0.98 (2)	0.98 (2)	0.98 (2)	0.98 (2)
H <sub>SF</sub> [Oe]	87.0 (1)	-	-	-	-
H <sub>SF</sub> <sup>N</sup> [Oe]	-	14.7 (2)	16.2 (2)	14.4 (1)	14.8 (1)
H <sub>SF</sub> <sup>H</sup> [Oe]	-	14.9 (2)	23.0 (2)	10.4 (2) / 1.4 (3)	-

To simplify the comprehension of the spectral analysis, Figure 3 shows the breakdown of the Mn-MNP EPR spectrum obtained at pH 4.8 at 40°C after 60 min of reaction, with the corresponding fitting and the residual curve. As observed, there is an excellent agreement between the data and the fitted values. In the bottom-panel, each component of the spectra is presented separately, corroborating that this technique allows for both the identification of all free-radical formed and their quantification (by comparing the intensity signals of each radical contributions to the Mn<sup>2+</sup> pattern sample). Since DMPO/•CH<sub>3</sub> radicals are formed as a consequence of the reaction between the •OH radical with the DMSO, the total [•OH] was calculated as the contribution of the intensities of the •OH signal plus the •CH<sub>3</sub> signal. Moreover, as the •N radical contribution was present in all spectra with similar area, including the blank sample, it was not considered in the discussion.

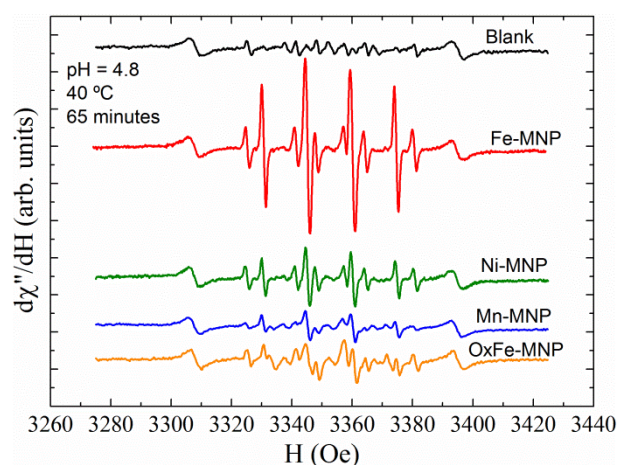


**Figure 2.** EPR spectra of DMPO spin-adducts obtained with Fe-MNP, Ni-MNP, Mn-MNP and oxFe-MNP nanoparticles in DMPO/DMSO containing solutions after H<sub>2</sub>O<sub>2</sub> addition. Top spectrum corresponds to the blank solution (without nanoparticles). Data was measured 65 min after H<sub>2</sub>O<sub>2</sub> addition at T= 40°C in pH = 4.8.

The [•OH] and [•OOH] measured for each ferrite (T = 40°C, pH = 4.8) are shown in Figure 4. This figure corresponds to the qualitative features observed in Figure 2; *i.e.* the catalytic activity of the Fe-MNP considering the [•OH] is remarkably higher than the observed for the other nanoparticle samples. The Fe-MNPs enhance the production of the [•OH] free radical by a factor of ~10 when compared to the blank

solution. As can be observed in Figure 2, the oxidized form of magnetite (oxFe-MNP) presents a reduction of EPR intensities that was further reflected as a strong decreased of  $[\bullet\text{OH}]$  as calculated in fig. 4, related to the smaller  $\text{Fe}^{2+}$  content in this sample.

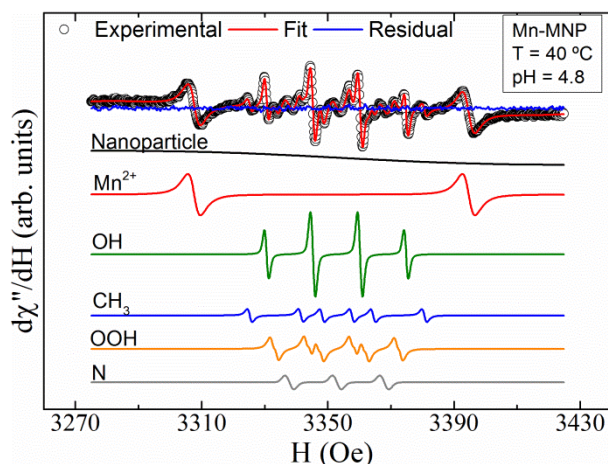


**Figure 3.** EPR spectrum and the corresponding fitting with the residual obtained for the Mn-MNP sample in DMPO/DMSO containing solution measured 60 min after addition of  $\text{H}_2\text{O}_2$  at  $T = 40^\circ\text{C}$  in  $\text{pH} = 4.8$  (top curve). Each DMPO-adduct radical component of the fitted spectra is shown separately in the spectra below (continuous line).

The solutions containing Mn and Ni nanoparticles also displayed higher values of  $[\bullet\text{OH}]$  compared to the blank solution; yet these values were lower than the values obtained for the solution with the Fe-MNP. Nevertheless, the  $[\bullet\text{OH}]$  was strongly reduced in the Mn-MNP relative to the Fe-MNP samples, while the levels of  $[\bullet\text{OOH}]$  were comparable between them. On the other hand, in the solution containing Ni-MNP, the amount of both radicals was reduced. These results confirm the crucial role played by the  $\text{Fe}^{2+}$  in the formation of  $\bullet\text{OH}$  radicals, since  $\text{Fe}^{2+}$  was oxidized (oxFe-MNP) or substituted by Mn and Ni ions in the Mn-MNP and the Ni-MNP samples, respectively. Figure S6 of the supplementary information shows the catalytic activity of each ferrite sample in

terms of the free radical  $\bullet\text{OH}$  defined as the  $[\bullet\text{OH}]$  produced in each sample divided by the  $[\bullet\text{OH}]$  obtained in the blank solution. Regarding the temporal evolution, no changes in radical production were observed in this catalytic activity of each ferrite in the first 120 minutes of reaction. When experiments were performed in  $\text{pH} = 7.4$ , as shown in Figure S7 of the supplementary information, there were no significant differences in the catalytic activity of the samples and the blank, indicating the absence of peroxidase-like activity at this pH.

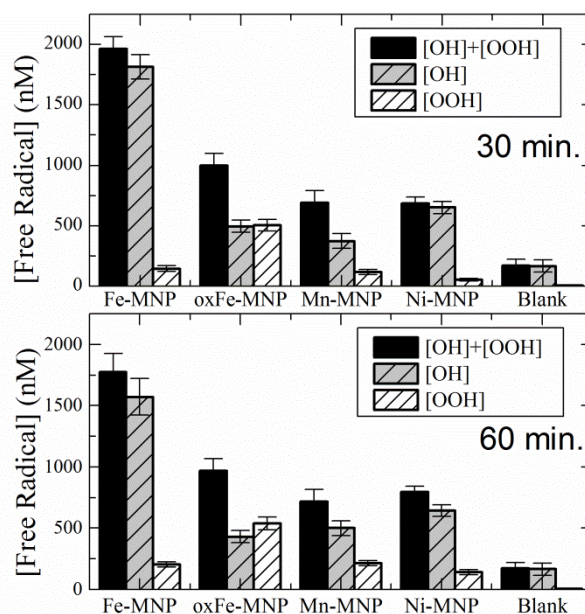


**Figure 4.** Total concentration of free radicals generated at 30 min. and 60 min. after addition of  $\text{H}_2\text{O}_2$  to a DMPO/DMSO in acetate buffer solution (black bar) calculated as the sum of  $[\bullet\text{OH}]$  and  $[\bullet\text{OOH}]$  for each ferrite sample and the blank, at  $40^\circ\text{C}$  in  $\text{pH} = 4.8$ . The error bars refer to the standard errors.

Quantitative analysis of the total  $[\bullet\text{OOH}]$  produced by the samples is hard, due to the limitations imposed by the DMPO/ $\bullet\text{OOH}$  adduct, even in the presence of DMSO as stabilizer. Nevertheless, a comparative study among the samples is valid and it indicates that the oxidation of the Fe-MNP (oxFe-MNP) and the incorporation of Mn leads to

an increase in the [ $\bullet\text{OOH}$ ]/[ $\bullet\text{OH}$ ] ratio when compared to the other two samples. It also shows that part of the DMPO/ $\bullet\text{OH}$  adduct detected arises from the decomposition of the DMPO/ $\bullet\text{OOH}$  adduct<sup>28-30</sup>. As expected, [ $\bullet\text{OOH}$ ] (related to the  $\text{Fe}^{3+}$  content) for oxFe-MNP, even underestimated, increases compared to the Fe-MNP sample. The [ $\bullet\text{OOH}$ ]/[ $\bullet\text{OH}$ ] ratio also increases for the Mn-MNP in comparison to the ratio of the Fe-MNP sample; yet not in the same magnitude as the observed for the sample oxFe-MNP, denoting the possibility of some activity of the Mn ion in the production of this free radical species.

To elucidate the effect of the different surface metallic ions in the nanoparticle's catalytic activity, we studied the free radical formation by EPR in the presence of anionic ligands that form different complexes with the metallic ions, similar to that used to study the catalytic activity of other nanomaterials<sup>43</sup>. For this purpose, we have used the  $\text{K}_3\text{PO}_4$  and 1,10-phenanthroline as anionic ligands. It is known that phosphate ions have strong affinity for  $\text{Fe}^{3+}$  ions,<sup>44</sup> and hence, they are able to coordinate with the  $\text{Fe}^{3+}$  ions in the nanoparticle surface. An effective interaction with both Fe ions is expected, yet it would be weaker with  $\text{Fe}^{2+}$  ions than with  $\text{Fe}^{3+}$  ions.<sup>31</sup> Phosphates also have some coordination ability with manganese and nickel ions,<sup>45</sup> although lower than the one observed with  $\text{Fe}^{3+}$  ions. In the case of the 1,10-phenanthroline compound, this has stronger affinity for  $\text{Ni}^{2+}$  and  $\text{Fe}^{2+}$  ions<sup>46</sup> and lower affinity for  $\text{Mn}^{2+}$  ions<sup>47,48</sup>. Figure 5 shows the [ $\bullet\text{OH}$ ] and [ $\bullet\text{OOH}$ ], after 60 minutes of reaction, obtained from the EPR fitting procedure using both ligands for all ferrite samples. As explained before, the solutions were prepared by dispersing the nanoparticles in acetate buffer at  $\text{pH} = 4.8$  containing phosphate (0.1 M) or 1,10-phenanthroline (0.1 M). Fig. S9 of the supplementary information gives the temporal dependence of total

concentration of radicals for the samples in presence of both ligands. In the case of the Fe-MNP with the phosphate ligands, a strong reduction of the [ $\bullet\text{OH}$ ], from  $\sim 2000$  nM to  $\sim 600$  nM was observed. For the other two samples, Mn-MNP and Ni-MNP, a reduction was also observed but less pronounced: from  $\sim 450$  nM to 300 nM for the Mn-MNP sample and from  $\sim 500$  nM to  $\sim 250$  nM for the Ni-MNP sample. When the 1,10-phenanthroline ligand was added to the solution, a strong reduction in the [ $\bullet\text{OH}$ ] was obtained for all samples. It is known that the functionalization of the nanoparticle's surface with anionic ligands with strong affinity for metallic cations changes the peroxidase-like activity in the ferrite nanoparticles<sup>45</sup>. Specifically, our results indicate that the use of anionic ligands with strong affinity for iron oxides can inhibit the peroxidase-like activity of ferrites where one of Fe ions dominates.

Since the phosphate and the 1,10-phenanthroline are scavengers of the  $\bullet\text{OH}$ , it is expected that they would stabilize the DMPO/ $\bullet\text{OOH}$  adduct. Considering this, the [ $\bullet\text{OOH}$ ] also decreases in presence of the phosphate in both the Fe-MNP and Ni-MNP sample when compared to the acetate buffer solution, whereas it is doubled for the Mn-MNP sample. For the 1,10-phenanthroline ligand, no contribution of the  $\bullet\text{OOH}$  species was observed for the Fe-MNP and Ni-MNP samples. For the Mn-MNP sample, a similar amount of [ $\bullet\text{OOH}$ ] was observed in 1,10-phenanthroline and in acetate buffer solution. These results suggest that the Mn ions in our ferrite nanoparticles present some catalytic activity increasing the [ $\bullet\text{OOH}$ ] radical in physiological conditions, which is not completely unexpected since the catalytic activity of Mn ions in oxides has been reported.<sup>49</sup>

Concerning the temperature dependence of the catalytic activity of the nanoparticles, Figure S8 in the supplementary information

compares the  $[\bullet\text{OH}]$  and  $[\bullet\text{OOH}]$  for sample Fe-MNP measured at 25°C and 40°C at pH = 4.8 for different times, showing that the

increment with the temperature is only about 10 %, which is not as significant as the changes in the particle composition or the pH.

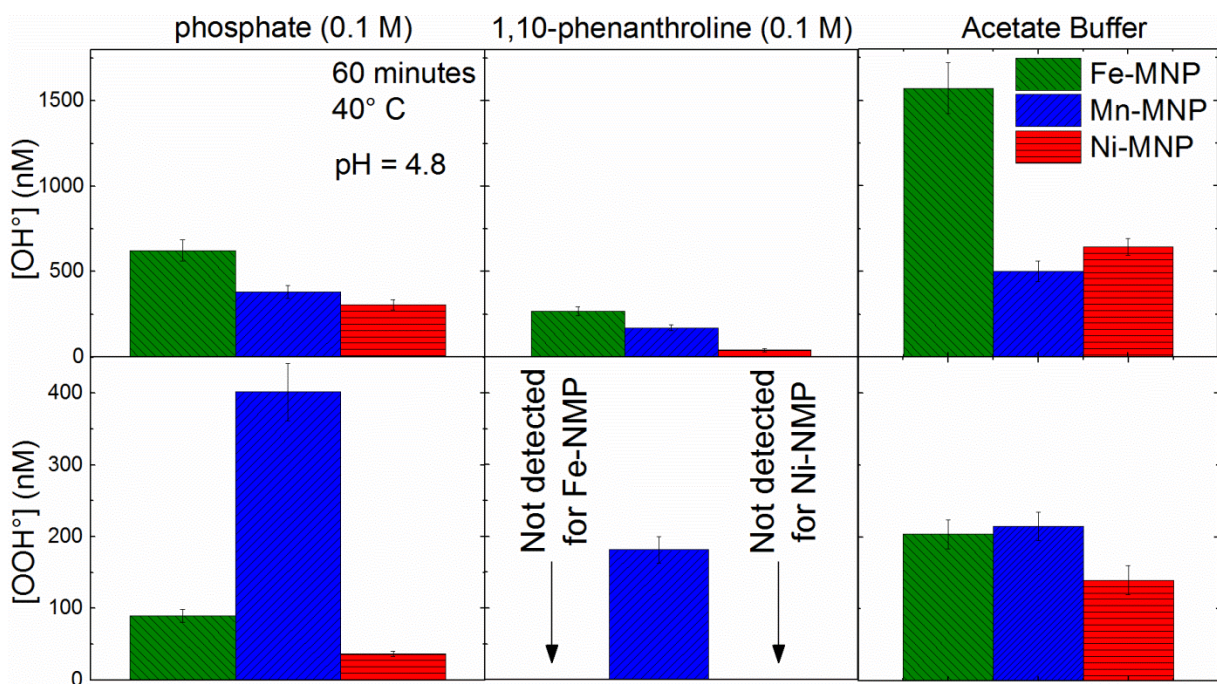


**Figure 5.** The  $[\bullet\text{OH}]$  and  $[\bullet\text{OOH}]$  obtained from the EPR fitting procedure for every ferrite sample measured at 40°C and in acetate buffer (pH 4.8) containing 0.1 M of phosphate, 0.1 M of 1,10-phenanthroline, and in only acetate buffer as a control. Reaction time of 60 min. The error bars refer to the standard errors.

### In-vitro experiments

Figure 6 gives the relative ROS production in BV2 cells exposed to 50  $\mu\text{g}/\text{mL}$  of oxFe-MNP, Ni-MNP or Mn-MNP, and incubated at 37°C and 40°C for 60 minutes. Additionally, the negative (without nanoparticles or TBHP) and positive (20  $\mu\text{M}$  THBP) controls at the two temperatures are shown. The procedure used to coat Fe-MNP with dextran is analogous to the protocol to produce the oxidized oxFe-MNPs. Also, Mn-MNP and Ni-MNP samples were coated with dextran for in vitro experiments, hence possible oxidation of  $\text{Ni}^{2+}$  and  $\text{Mn}^{2+}$  cannot be ruled out.

For the experiments performed at 37°C, the ROS levels measured for the nanoparticles

cannot be considered statistically different from the positive control. Yet, the oxFe-MNP sample presents a ROS level slightly higher than the samples of Mn-MNP and Ni-MNP. This tendency is similar to that observed for the catalytic activity determined for each sample in the EPR measurements. Comparing the ROS level for the in vitro experiments at 37°C, the relation oxFe-MNP:Mn-MNP:Ni-MNP = 1:0.79:0.78 is obtained. The relation 1:0.77:0.86 is obtained for the total amount of free radicals in the EPR experiments at 60 minutes of reaction.

Incubation of cells at 40°C for one hour increased ROS production in both the control and the experimental groups, mostly due to the enhancement of cell stress at a this high temperature. A stable increment in the



measured levels of ROS is observed for the negative control in comparison to the value at 37°C, which is close to the value obtained for the positive control. In fact, comparing both controls, the obtained value cannot be taken as statistically different despite a tendency of having a higher value in the positive control as indicated. However, the ROS levels measured for oxFe-MNP and Ni-MNP are similar and statistically higher than that of the negative control. Interestingly, the Mn-MNP sample showed considerably higher ROS activity than the other samples, as well as a higher activity than the positive control at the same temperature.

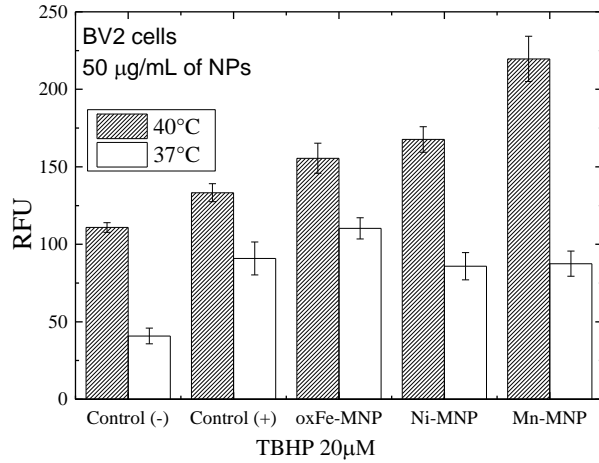
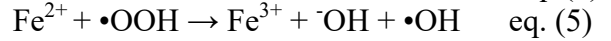
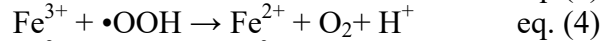
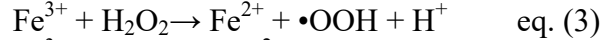
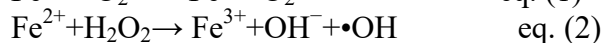
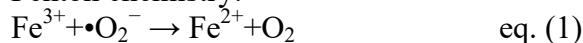


**Figure 6.** Intracellular ROS levels (in relative fluorescence units) of BV2 cells exposed to 50 µg/mL of oxFe-MNP, Ni-MNP and Mn-MNP at 37 °C (white bars) and 40 °C (dashed bars). The bars from negative control (-) and positive control with 20 µM of TBHP (+) are also included ( $p > 0.05$ ).

## Discussion

Formation  $\bullet\text{OH}$  is the critical point concerning the toxicity associated to the peroxidase-like activity of ferrite nanoparticles, and it is iron-catalyzed by the Haber–Weiss reaction, which makes use of Fenton chemistry.<sup>50,51</sup>



The Haber–Weiss reaction chain has different starting points, one related to the direct reaction of the  $\text{Fe}^{2+}$  with the  $\text{H}_2\text{O}_2$ , and other related to a previous reduction of the  $\text{Fe}^{3+}$  to  $\text{Fe}^{2+}$ . This is an interesting point, since an oxidation of the nanoparticle surface Fe it is expected when the nanoparticles are in aqueous solution or during the functionalization process with Dextran; however, free radicals can be also produced starting from the reaction described in eq. (1) and eq. (3), but considering that the chain reaction starting from eq. (1) has a faster kinetics.

It is expected that the peroxidase-like activity of the ferrite nanoparticles depends on their surface-to-volume ratio. Indeed, Gao *et al.*<sup>8</sup> reported that the catalytic reaction of ferrite diminishes with increasing particle size. In addition to the surface area, other factors related to the surface of the iron oxide are important to determine the peroxidase-like activity of the iron oxides. The ability to the binding and the dissociation of the oxygen molecules to the surface of the particles is critical factors with a complexity; for stance, in molecules with an active Fe ion in the core, the dioxygen binding and dissociation dynamics of the resulting iron peroxide species are key points for the catalytic activity of molecule<sup>52</sup>. Besides the surface, the structure and superficial plane are also important in the peroxidase-like of oxides with spinel structure, including the maghemite and the magnetite<sup>53</sup>, among others 3d transition metal oxides with similar structure<sup>54</sup>. Following, the surface reduction and oxidation kinetics in the oxide system also play fundamental roles in the catalytic activity of the metal oxide systems, as studied by Righi *et al.*<sup>55</sup>. These authors showed

theoretically that the vacancies are a determining factor for the oxidation/reduction reactions in the (100) plane of the maghemite, which can be related with the Haber-Weiss chain reactions through the reaction described in eq. (1). In addition, Xiaoyu Wang *et al.*<sup>56</sup> showed recently that the population of  $e_g$  orbitals plays a fundamental role in the peroxidase-like catalytic activity of perovskite oxide-based nanosystems.

As discussed above, prediction of the peroxidase-like activity of the ferrite nanoparticles are complex and involve several physical-chemical factors. Nevertheless, a deeper analyzes of our results allows to investigate the role of the surface chemical catalytic activity among the different ferrites studied, with respect to the production of the  $\bullet\text{OH}$  radical as determined by EPR ( $[\bullet\text{OH}]_{\text{EPR}}$ ). For this, we firstly consider the influence of the particle size by normalizing  $[\bullet\text{OH}]_{\text{EPR}}$  for each sample with the surface to volume ratio weighted by the size distribution as obtained from TEM analyzes (*i.e.*  $[\pi d_{\text{TEM}}^2]/[(\pi/6)d_{\text{TEM}}^3]*f(d)$ ). Here, we assume that the atoms acting in the catalytic reaction are localized in the last atomic layer: the superficial plane. We also normalize  $[\bullet\text{OH}]_{\text{EPR}}$  with the  $[\text{Fe}^{2+}]/[\text{Fe}]$  ratio obtained from the XPS results. This normalized amount was defined by the parameter  $R^{\text{OH}}$  as follows:

$$R^{\text{OH}} = \frac{[\bullet\text{OH}]_{\text{EPR}} \times ((\pi d_{\text{TEM}}^2) / ((\pi/6) d_{\text{TEM}}^3) * f(d))}{[\text{Fe}^{2+}] / [\text{Fe}]} \quad \text{eq. (7)}$$

Figure 7 presents the  $R^{\text{OH}}$  values calculated from the EPR results at 30 and 60 minutes of reaction for samples Fe-MNP, oxFe-MNP,

Ni-MNP and Mn-MNP. Despite the error bars, due mainly to the size dispersion, the resulting values for the formation of  $\bullet\text{OH}$  indicate the key role played by the  $\text{Fe}^{2+}$  by the almost constant value of  $R^{\text{OH}}$  after normalization, excepting for sample Mn-MNP that presents a smaller  $R^{\text{OH}}$  value.

The substitution of  $\text{Fe}^{2+}$  by Mn and Ni ions in the spinel structure reduces the catalytic activity that produces the free radical  $\bullet\text{OH}$ . In fact, the Mn-MNP sample showed a lower amount of  $[\bullet\text{OH}]$  than expected. Probably, this is related to a competitive catalytic reaction involving the Mn ions and the free radical  $\bullet\text{OOH}$ . This Mn activity is indicated by the EPR measurements in presence of phosphate and 1,10-phenanthroline. As mentioned before, the phosphate anion and the  $\text{Fe}^{2+}$  form a complex in the surface of the nanoparticles, leading to a strong reduction in the amount of radical  $[\bullet\text{OH}]$  in the solution of Fe-MNPs. As expected, the reduction of  $[\bullet\text{OH}]$  was not that marked in the Ni-MNP and Mn-MNP samples, due to the lower concentration of  $\text{Fe}^{2+}$  in these nanoparticles. This result may indicate that the Mn ions catalyze the production of the  $[\bullet\text{OOH}]$  radical. The catalytic activity of  $\text{Mn}^{3+}$  ion with  $e_g$  hybridization is reported in the literature.<sup>49,56</sup> Despite the fact that our results clearly indicate the role in the peroxidase-like catalytic activity of  $\text{Fe}^{2+}$  and  $\text{Fe}^{3+}$  in the octahedral site of the ferrites, deeper studies on the structure and the cationic distribution in the spinel structure must be performed in order to fully elucidate the activity of all cations in this chemical reaction.

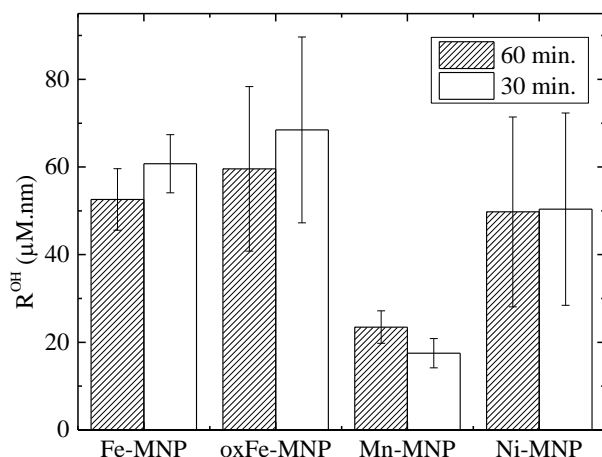


**Figure 7.** Quantity  $R^{\text{OH}}$  calculated with eq. (4) from the value of  $[\bullet\text{OH}]$  determined by EPR at 30 and 60 minutes of reaction,  $\text{pH} = 4.8$  and  $T = 40^\circ\text{C}$ , using the respective  $[\text{Fe}^{2+}]/[\text{Fe}]$  ratio estimated from the XPS results and the average surface calculated from the diameter distribution obtained from TEM analyzes. The error bars refer to the calculated dispersion.

Concerning the *in vitro* cell culture results, we emphasize that the catalytic activity as inferred from EPR data and fluorescence *in vitro* should be compared with caution. Not only do EPR and photoluminescent protocols have different specificities, but they were measured in different conditions. It is important to mention other remarkable differences between the ROS level determined in the *in vitro* experiments and EPR quantification of the free radicals produced. First, the oxidative stress of the cell and the influence on its metabolism should be taken into account, as shown by the ROS level measured for the negative and positive controls in the *in vitro* experiments at  $40^\circ\text{C}$ . Second, the acetate buffer used in the EPR experiments was different from the carbonate buffer used in the culture media or the phosphate-rich media in intracellular localization. In the proximity of these chelates of transition metals, the process could lead to the formation of metallic complexes on the surface of the

nanoparticles, directly affecting the catalytic activity of the nanoparticles.<sup>45</sup> Third, the concentration of nanoparticles used in the EPR measurements was  $\sim 600 \mu\text{g/mL}$ , while in cell culture experiments this concentration would have induced toxicity issues. At the same time, the kinetics of the reactions should also be taken into consideration since EPR, photoluminescent protocols involve very different time scales (seconds and hours, respectively), and hence, direct comparison of data from both techniques would require additional experiments to evaluate the time evolution of the reactive species production in each media with the same particle concentration. Fourth, our Dextran-coated nanoparticles tend to be localized in the lysosome<sup>57</sup> ( $\text{pH} = 4.8$ ), but different coatings may result in other areas of different pH conditions (e.g.,  $\text{pH} 7.4$ ), where the ferrites displayed no catalytic activity in the EPR experiments. Therefore, it is important to know the intracellular localization of the nanoparticles in the cell for a better comparison with the EPR studies. Finally, we remark the procedure used to obtain the coating is also important, since it may result in the oxidation (or in other cases the reduction) of the metallic ions in the surface of the particles. Our procedure to obtain the Dextran-coated nanoparticles results in the oxidation of  $\text{Fe}^{2+}$  ions, affecting directly the catalytic activity, and probably the Ni and Mn ions are also affected in this process. Thus,

deeper studies are necessary for a better compression of this point. Despite this, we found a relatively good correspondence between in vitro and EPR experiments, with both indicating a catalytic activity of the nanoparticles that increases the amount of ROS. These results are relevant for the applications of ferrite nanoparticles in biomedical protocols, and they indicate that the composition and the oxidation state of the nanoparticles are critical. The EPR is a useful technique to evaluate the activity of the nanoparticles, and it can complement the in vitro evaluations.

For the Mn-MNP, the higher ROS levels detected for in vitro experiments are probably related to the amount of radical  $\bullet\text{OOH}$  produced, including the catalytic activity of  $\text{Mn}^{3+}$  ion present in the sample that is not correctly detected by EPR using DMPO as a spin-trap. Concerning the Mn ferrite, more detailed studies on the Mn ionic valence, its distribution in the crystalline sites of the ferrite and the correct measurement of the  $[\bullet\text{OOH}]$  produced using another spin-trap specific for this radical, are needed.

## Conclusions

From the EPR measurements, we were able to quantify the formation of  $[\bullet\text{OH}]$  and  $[\bullet\text{OOH}]$  resulting from the catalytic activity (pH = 4.8 and 40 °C) of the Mn-MNP, Ni-MNP and Fe-MNP and its oxidized form (oxFe-MNP). Our results indicate that the production of the  $[\bullet\text{OH}]$  radical was triggered by the presence of  $\text{Fe}^{2+}$ . Because of this, the total amount of free radical produced by the catalytic activity of the nanoparticles was reduced when Mn and Ni ions were used to substitute  $\text{Fe}^{2+}$  in the ferrite crystal lattice. Accordingly, lower concentration of this radical was also observed in the oxidized magnetite. No radical formation was evidenced for any sample at pH = 7.4. In vitro measurements of ROS formation in BV2 cells

exposed to the dextran-coated nanoparticles at 37 °C and 40°C showed measurable catalytic activity of the nanoparticles. For 37°C, in vitro results are in conformity with the EPR experiments.

An additional outcome stemming from the above results is the significance of keeping the experimental conditions as invariable as possible if direct comparison between different techniques is made. Nanoparticles with high peroxidase-like catalytic activity could be of interest for oncological applications, whereas, for magnetic resonance imaging, ophthalmology or drug delivery, the design of MNPs with minimum peroxidase-like activity is desired. Therefore, the control of surface oxidation or functionalization is a key issue for a safe and efficient design of these materials. We believe that our work provides a basic outline to better engineer and produce ferrite nanoparticles with predictable catalytic impact on desired applications, regardless of whether these applications are in the field of biomedicine, industry or environmental sciences.

## Supporting Information

The following files are available free of charge. Supporting information shows the fitted Fe-2p<sub>3/2</sub> and the 3p XPS spectra of samples Fe-MNP, Mn-MNP and Ni-MNP; including the respective tables with main parameters obtained from the XPS analyses, UV-visible spectrophotometry results, concentration of the Free Radicals of the different samples as a function of the reaction time measured by EPR, the concentration of free radicals as function of time reaction measured by EPR for sample Fe-MNP at different temperatures (25°C and 40°C) and pH (4.8 and 7.0), and the time dependence of  $[\bullet\text{OH}]$  and  $[\bullet\text{OOH}]$  for samples Fe-MNP, Mn-MNP and Ni-MNP in acetate buffer (pH 4.8) containing 0.1 M of phosphate and 1,10-phenanthroline.



## AUTHOR INFORMATION

### Corresponding Author

\*corresponding author: lima@cab.cnea.gov.ar

### Present Addresses

† A. C. Moreno Maldonado is now working in the Instituto de Nanociencias de Zaragoza (Spain), M. L. Mojica Piscioti in the International Research Clinical Center of St Anne's University Hospital Brno (Czech Republic) and L. M. Rodríguez in ESISNA group, Instituto de Ciencia de Materiales de Madrid (ICMM - CSIC), Sor Juana Inés de la Cruz 3, 28049, Madrid, Spain.

### Author Contributions

The manuscript was written through contributions of all authors. All authors have given approval to the final version of the manuscript. ‡ These authors contributed equally.

### Funding Sources

The authors are also grateful for the received financial support from the Argentinian agency ANPCyT (Project No PICTs 2014-2612, 2015-0883 and 2016-0288), EU-commission: H2020-MSCA-RISE-2016 SPICOLST PROJECT No 734187, and from the Spanish Ministerio de Economía y Competitividad (MINECO) through project MAT2016-78201-P and the Aragon Regional Government (DGA, Project No. E26).

### ACKNOWLEDGMENT

Authors are grateful to the Surface group and the Metal group from the Centro Atómico Bariloche for the use of the XPS spectrophotometer and the TEM microscope, respectively. The authors are also indebted with Dr. Alejandro Butera for critical reading and suggestions. Alfonso Toro Córdova is indebted with Mexican CONACyT for his post-doctoral fellowship (CVU 257448) at

INA, Zaragoza. Dra M Raineri and Dr. T. E. Torres are indebted with the Argentinian CONICET for her Post-doctoral fellowship, and Dra M. L. Mojica Piscioti and A. C. Moreno Maldonado are indebted with the Argentinian CNEA for their post-doctoral and magister fellowships, respectively.

### REFERENCES

- (1) Bobo, D.; Robinson, K. J.; Islam, J.; Thurecht, K. J.; Corrie, S. R. Nanoparticle-Based Medicines: A Review of FDA-Approved Materials and Clinical Trials to Date. *Pharm Res-Dordr* **2016**, *33*, 2373-2387.
- (2) Schutz-Sikma, E. A.; Joshi, H. M.; Ma, Q.; MacRenaris, K. W.; Eckermann, A. L.; Dravid, V. P.; Meade, T. J. Probing the Chemical Stability of Mixed Ferrites: Implications for Magnetic Resonance Contrast Agent Design. *Chem. Mater.* **2011**, *23*, 2657-2664.
- (3) Saldívar-Ramírez, M. M. G.; Sánchez-Torres, C. G.; Cortes-Hernández, D. A.; Escobedo-Bocardo, J. C.; Almanza-Robles, J. M.; Larson, A.; Resendiz-Hernández, P. J.; Acuna-Gutiérrez, I. O. Study on the Efficiency of Nanosized Magnetite and Mixed Ferrites in Magnetic Hyperthermia. *J. Mater. Sci.-Mater. M.* **2014**, *25*, 2229-2236.
- (4) Pereira, M. C.; Oliveira, L. C. A.; Murad, E. Iron Oxide Catalysts: Fenton and Fenton-Like Reactions - A Review. *Clay Miner.* **2012**, *47*, 285-302.
- (5) Weiwei, H.; Wamer, W.; Qingsu, X.; Jun-jie, Y.; Fu, P. P. Enzyme-Like Activity of Nanomaterials. *J. Environ. Sci. Health C* **2014**, *32*, 186-211.
- (6) Hermanek, M.; Zboril, R.; Medrik, N.; Pechousek, J.; Gregor, C. Catalytic Efficiency of Iron(III) Oxides in Decomposition of Hydrogen Peroxide: Competition Between the Surface Area and Crystallinity of Nanoparticles. *J. Am. Chem. Soc.* **2007**, *129*, 10929-10936.
- (7) Wang, B.; Yin, J. J.; Zhou, X. Y.; Kurash, I.; Chai, Z. F.; Zhao, Y. L.; Feng, W. Y. Physicochemical Origin for Free Radical Generation of Iron Oxide Nanoparticles in Biomicroenvironment: Catalytic Activities Mediated by Surface Chemical States. *J. Phys. Chem. C* **2013**, *117*, 383-392.
- (8) Gao, L. Z.; Zhuang, J.; Nie, L.; Zhang, J. B.; Zhang, Y.; Gu, N.; Wang, T. H.; Feng, J.; Yang, D. L.; Perrett, S.; et al. Intrinsic Peroxidase-Like Activity of Ferromagnetic Nanoparticles. *Nat. Nanotechnol.* **2007**, *2*, 577-583.
- (9) Lin, W. B. Introduction: Nanoparticles in Medicine. *Chem. Rev.* **2015**, *115*, 10407-10409.
- (10) Iranmanesh, M.; Hulliger, J. Magnetic Separation: Its Application in Mining, Waste Purification,

- Medicine, Biochemistry and Chemistry. *Chem. Soc. Rev.* **2017**, *46*, 5925-5934.
- (11) Gobbo, O. L.; Sjaastad, K.; Radomski, M. W.; Volkov, Y.; Prina-Mello, A. Magnetic Nanoparticles in Cancer Theranostics. *Theranostics* **2015**, *5*, 1249-1263.
- (12) Gumpelmayer, M.; Nguyen, M.; Molnar, G.; Bousseksou, A.; Meunier, B.; Robert, A. Magnetite Fe<sub>3</sub>O<sub>4</sub> Has no Intrinsic Peroxidase Activity, and Is Probably not Involved in Alzheimer's Oxidative Stress. *Angew. Chem. Int. Edit.* **2018**, *57*, 14758-14763.
- (13) Yu, F.; Huang, Y.; Cole, A. J.; Yang, V. C. The Artificial Peroxidase Activity of Magnetic Iron Oxide Nanoparticles and Its Application to Glucose Detection. *Biomaterials* **2009**, *30*, 4716-4722.
- (14) Costa, R. C. C.; Lelis, M. F. F.; Oliveira, L. C. A.; Fabris, J. D.; Ardisson, J. D.; Rios, R. R. V. A.; Silva, C. N.; Lago, R. M. Novel Active Heterogeneous Fenton System Based on Fe<sub>3-x</sub>M<sub>x</sub>O<sub>4</sub> (Fe, Co, Mn, Ni): The Role of M<sup>2+</sup> Species on the Reactivity Towards H<sub>2</sub>O<sub>2</sub> Reactions. *J. Hazard Mater.* **2006**, *129*, 171-178.
- (15) Elmaci, G.; Frey, C. E.; Kurz, P.; Zümreoğlu-Karan B. Water Oxidation Catalysis by Using Nano-Manganese Ferrite Supported 1D-(Tunnelled), 2D-(Layered) and 3D-(Spinel) Manganese Oxides. *J. Mater. Chem. A* **2016**, *4*, 8812-8821.
- (16) Goyal, A.; Bansal, S.; Samuel, P.; Kumard, V.; Singhal S. CoMn<sub>0.2</sub>Fe<sub>1.8</sub>O<sub>4</sub> Ferrite Nanoparticles Engineered by Sol-Gel Technology: an Expert and Versatile Catalyst for the Reduction of Nitroaromatic Compounds. *J. Mater. Chem. A* **2014**, *2*, 18848-18860.
- (17) Wang, H.; Li, S.; Si, Y.; Sun, Z.; Li, S.; Lin, Y. Recyclable Enzyme Mimic of Cubic Fe<sub>3</sub>O<sub>4</sub> Nanoparticles Loaded on Graphene Oxide-Dispersed Carbon Nanotubes with Enhanced Peroxidase-Like Catalysis and Electrocatalysis. *J. Mater. Chem. B* **2014**, *2*, 4442-4448.
- (18) Shi, W. B.; Zhang, X. D.; He, S. H.; Huang, Y. M. CoFe<sub>2</sub>O<sub>4</sub> Magnetic Nanoparticles as a Peroxidase Mimic Mediated Chemiluminescence for Hydrogen Peroxide and Glucose. *Chem. Commun.* **2011**, *47*, 10785-10787.
- (19) Clerc, P.; Jeanjean, P.; Hallalli, N.; Gougeon, M.; Pipy, B.; Carrey, J.; Fourmy, D.; Gigoux, V. Targeted Magnetic Intra-Lysosomal Hyperthermia Produces Lysosomal Reactive Oxygen Species and Causes Caspase-1 Dependent Cell Death. *J. Control. Release* **2018**, *270*, 120-134.
- (20) Davies, M. J. Detection and Characterization of Radicals Using Electron Paramagnetic Resonance (EPR) Spin Trapping and Related Methods. *Methods* **2016**, *109*, 21-30.
- (21) Eaton, G. R.; Eaton, S. S.; Barr, D. P.; Weber, T. R. *Quantitative EPR*; Springer-Verlag:Wien, Germany, 2010.
- (22) Lund, A.; Shiotani M. *Applications of EPR in Radiation Research*; Springer International Publishing:Heidelberg, Germany, 2014.
- (23) Lund, A.; Shiotani, M.; Shimada, S. *Principles and Applications of ESR Spectroscopy*; Springer Science+Business Media B.V.:Heidelberg, Germany, 2011.
- (24) Saifutdinov, R. G.; Larina, L. I.; Vakulskaya, T. I.; Voronkov, M. G. *Electron Paramagnetic Resonance in Biochemistry and Medicine*; Kluwer Academic Publishers:New York, USA, 2002.
- (25) Fainstein, C.; Winkler, E.; Saravi, M. ESR/Alanine  $\gamma$ -Dosimetry in the 10-30 Gy Range. *Appl. Radiat. Isot.* **2000**, *52*, 1195-1196.
- (26) Winkler, E.; Etchegoin, P.; Fainstein, A.; Fainstein, C. Luminescence and Resonant Raman Scattering of Color Centers in Irradiated Crystalline L-Alanine. *Phys. Rev. B* **1998**, *57*, 13477-13484.
- (27) Chen, Z. W.; Yin, J. J.; Zhou, Y. T.; Zhang, Y.; Song, L.; Song, M. J.; Hu, S. L.; Gu, N. Dual Enzyme-like Activities of Iron Oxide Nanoparticles and Their Implication for Diminishing Cytotoxicity. *ACS Nano* **2012**, *6*, 4001-4012.
- (28) Saito, K.; Takahashi, M.; Kamibayashi, M.; Ozawa, T.; Kohno, M. Comparison of Superoxide Detection Abilities of Newly Developed Spin Traps in the Living Cells. *Free Radic. Res.* **2009**, *43*, 668-676.
- (29) Sanders, S. P.; Harrison, S. J.; Kuppusamy, P.; Sylvester, J. T.; Zweier, J. L. Comparative Study of EPR Spin Trapping and Cytochrome C Reduction Techniques for the Measurement of Superoxide Anions. *Free Radic. Biol. Med.* **1994**, *16*, 753-761.
- (30) Roubaud, V.; Sankarapandi, S.; Kuppusamy, P.; Tordo, P.; Zweier, J. L. Quantitative Measurement of Superoxide Generation Using the Spin Trap 5-(Diethoxyphosphoryl)-5-methyl-1-pyrroline-N-oxide. *Anal. Biochem.* **1997**, *247*, 404-411.
- (31) Aslamkhan, A. G.; Aslamkhan, A.; Ahearn, G. A. Preparation of Metal Ion Buffers for Biological Experimentation: A Methods Approach with Emphasis on Iron and Zinc. *J. Exp. Zool.* **2002**, *292*, 507-522.
- (32) Torres, T. E.; Lima Jr., E.; Mayoral, A.; Ibarra, A.; Marquina, C.; Ibarra, M. R.; Goya, G. F. Validity of the Néel-Arrhenius Model for Highly Anisotropic Co<sub>x</sub>Fe<sub>3-x</sub>O<sub>4</sub> Nanoparticles. *J. Appl. Phys.* **2015**, *118*, 183902.
- (33) Arelaro, A. D.; Lima Jr., E.; Rossi, L. M.; Kiyohara, P. K.; Re-chenberg, H. R. Ion Dependence of Magnetic Anisotropy in MFe<sub>2</sub>O<sub>4</sub> (M = Fe, Co, Mn) Nanoparticles Synthesized by High-Temperature Reaction. *J. Magn. Magn. Mater.* **2008**, *320*, E335-E338.
- (34) Grosvenor, A. P.; Kobe, B. A.; Biesinger, M. C.; McIntyre, N. S. Investigation of Multiplet Splitting of Fe 2p XPS Spectra and Bonding in Iron Compounds. *Surf. Interface Anal.* **2004**, *36*, 1564-1574.

- (35) Yamashita, T.; Hayes, P. Effect of Curve Fitting Parameters on Quantitative Analysis of  $\text{Fe}_{0.94}\text{O}$  and  $\text{Fe}_2\text{O}_3$  Using XPS. *J. Electron. Spectrosc.* **2006**, *152*, 6-11.
- (36) Hoppe, M. *Magnetic, Structural, and Electronic Properties of  $\text{NiFe}_2\text{O}_4$  Ultrathin Films – Volume 118*; Forschungszentrum Jülich GmbH: Jülich, Germany, 2016.
- (37) Shaju, K. M.; Ramanujachary, K. V.; Lofland, S. E.; Subba Rao, G. V.; Chowdari, B. V. R. Spectral, Magnetic and Electrochemical Studies of Layered Manganese Oxides With P2 and O2 Structure. *J. Mater. Chem.* **2003**, *13*, 2633-2640.
- (38) Yeh, J. J.; Lindau, I. Atomic Subshell Photoionization Cross Sections and Asymmetry Parameters :  $1 \leq Z \leq 103$ . *Atom. Data Nucl. Data* **1985**, *32*, 1-155.
- (39) Budaev, S. L.; Batoeva, A. A.; Tsybikova, B. A. Effect of Fenton-Like Reactions on the Degradation of Thiocyanate in Water Treatment. *J. Environ. Chem. Eng.* **2014**, *2*, 1907-1911.
- (40) Tobia, D.; Winkler, E. L.; Milano, J.; Butera, A.; Kempf, R.; Bianchi, L.; Kaufmann, F. Determination of Gd Concentration Profile in  $\text{UO}_2\text{-Gd}_2\text{O}_3$  Fuel Pellets. *J. Nucl. Mater.* **2014**, *451*, 207-210.
- (41) Chang, T.-T.; Foster, D.; Kahn, A. H. An Intensity Standard for Electron Paramagnetic Resonance Using Chromium Doped Corundum ( $\text{Al}_2\text{O}_3\text{:Cr}^{3+}$ ). *J. Res. Natl. Bureau Stand.* **1978**, *83*, 133.
- (42) Low, W. Hyperfine Structure and Nuclear Moments of Gadolinium from Paramagnetic Resonance Spectrum. *Phys. Rev.* **1956**, *103*, 1309.
- (43) Tarpani, L.; Bellezza, F.; Sassi, P.; Gambucci, M.; Cipiciani, A.; Latterini, L. New Insights into the Effects of Surface Functionalization on the Peroxidase Activity of Cytochrome c Adsorbed on Silica Nanoparticles. *J. Phys. Chem. B* **2019**, *123*, 2567-2575.
- (44) Li, P. H.; Lin, J. Y.; Chen, C. T.; Ciou, W. R.; Chan, P. H.; Luo, L. Y.; Hsu, H. Y.; Diao, E. W. G.; Chen, Y. C. Using Gold Nanoclusters As Selective Luminescent Probes for Phosphate-Containing Metabolites. *Anal. Chem.* **2012**, *84*, 5484-5488.
- (45) Chen, C. X.; Lu, L. X.; Zheng, Y.; Zhao, D.; Yang, F.; Yang, X. R. A New Colorimetric Protocol for Selective Detection of Phosphate Based on the Inhibition of Peroxidase-Like Activity of Magnetite Nanoparticles. *Anal. Methods* **2015**, *7*, 161-167.
- (46) Sigel, H.; Da Costa, C. P.; Song, B.; Carloni, P.; Gregan, F. Stability and Structure of Metal Ion Complexes Formed in Solution with Acetylphosphate and Acetylphosphonate: Quantification of Isomeric Equilibria. *J. Am. Chem. Soc.* **1999**, *121*, 6248-6257.
- (47) Martell, A.; Smith, R. *Critical Stability Constants*; Plenum Press: New York, USA, 1982.
- (48) Irving, H.; Mellor, D. H. Stability of Metal Complexes of 1,10-Phenanthroline and Its Analogues. Part I. 1,10-Phenanthroline and 2,2'-Bipyridyl. *J. Chem. Soc.* **1962**, 5222-5237.
- (49) Wariishi, H.; Valli, K.; Gold, M. H. Manganese(II) Oxidation by Manganese Peroxidase from the Basidiomycete Phanerochaete-Chrysosporium - Kinetic Mechanism and Role of Chelators. *J. Biol. Chem.* **1992**, *267*, 23688-23695.
- (50) Kehrer J. P. The Haber-Weiss Reaction and Mechanisms of Toxicity. *Toxicology* **2000**, *149*, 43-50.
- (51) Matavos-Aramyan S., Moussavi M. Advances in Fenton and Fenton-Based Oxidation Processes for Industrial Effluent Contaminants Control-A Review. *Int. J. Environ. Sci. Nat. Resour.* **2017**, *2*, 555594.
- (52) Du, L.; Liu, F.; Li, Y.; Yang, Z.; Zhang, Q.; Zhu, C.; Gao, J. Dioxygen Activation by Iron Complexes: The Catalytic Role of Intersystem Crossing Dynamics for a Heme-Related Model, *J. Phys. Chem. C* **2018**, *122*, 2821-2831.
- (53) Cheng, X. -L.; Jiang, J. -S.; Jiang, D. -M.; Zhao, Z. -J. Synthesis of Rhombic Dodecahedral  $\text{Fe}_3\text{O}_4$  Nanocrystals with Exposed High-Energy {110} Facets and Their Peroxidase-Like Activity and Lithium Storage Properties. *J. Phys. Chem. C* **2014**, *118*, 12588-12598.
- (54) Mu, J.; Zhang, L.; Zhao, G.; Wang, Y. The Crystal Plane Effect on the Peroxidase-Like Catalytic Properties of  $\text{Co}_3\text{O}_4$  Nanomaterials. *Phys. Chem. Chem. Phys.* **2014**, *16*, 15709-15716.
- (55) Righi, G.; Magri, R. Reduction and Oxidation of Maghemite (001) Surfaces: The Role of Iron Vacancies. *J. Phys. Chem. C* **2019**, *123*, 15648-15658.
- (56) Wang, X.; Gao, X. J.; Qin, L.; Wang, C.; Song, L.; Zhou, Y. -N.; Zhu, G.; Cao, W.; Lin, S.; Zhou, L.; et al.  $e_g$  Occupancy as an Effective Descriptor for the Catalytic Activity of Perovskite Oxide-Based Peroxidase Mimics. *Nat. Commun.* **2019**, *10*, 704.
- (57) Arbab, A. S.; Wilson, L. B.; Ashari, P.; Jordan, E. K.; Lewis, B. K.; Frank, J. A. A Model of Lysosomal Metabolism of Dextran Coated Superparamagnetic Iron Oxide (SPIO) Nanoparticles: Implications for Cellular Magnetic Resonance Imaging. *NMR Biomed.* **2005**, *18*, 383-389.